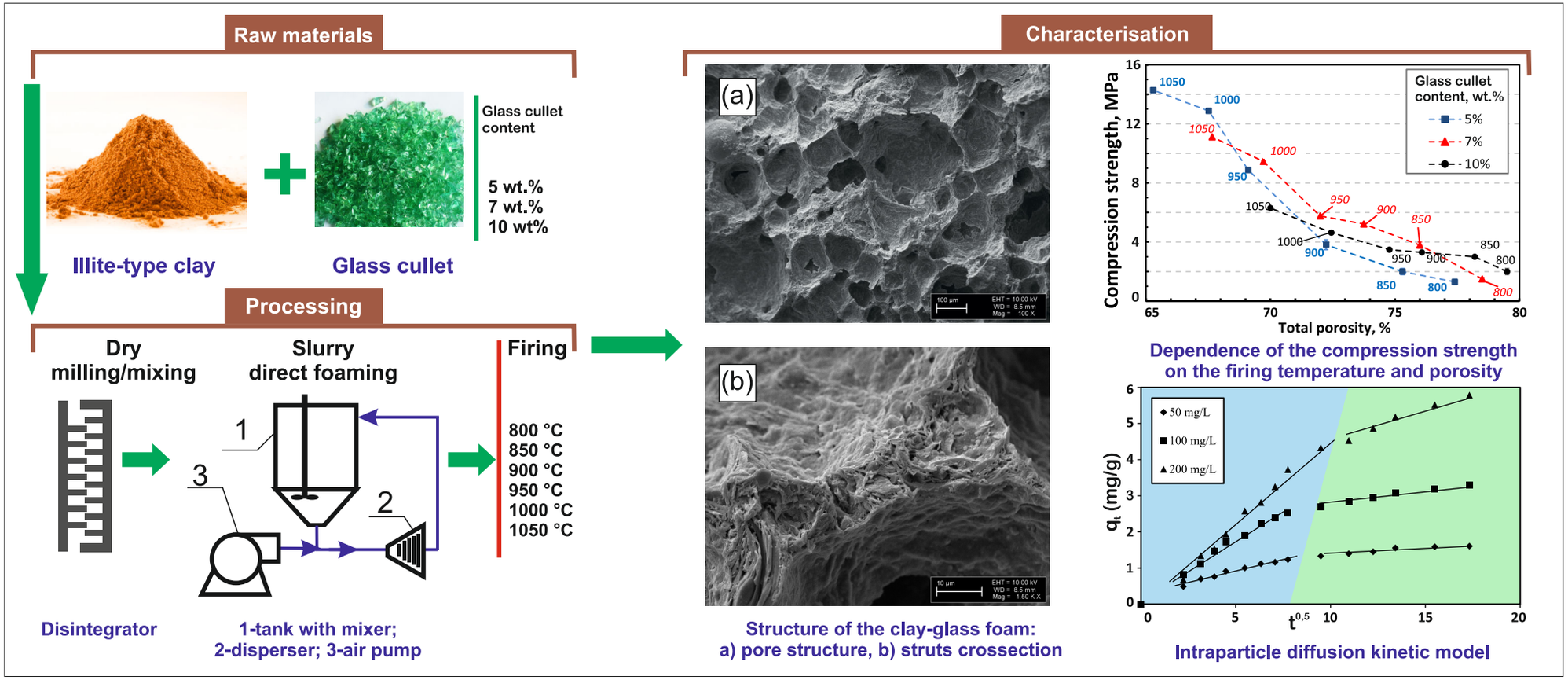
Raw materials
Glass cullet content
5 wt.%
7 wt.%
10 wt%
Illite-type clay
Glass cullet
Processing
Dry milling/mixing
Slurry direct foaming
Firing
800 °C
850 °C
900 °C
950 °C
1000 °C
1050 °C
1
2
3
Disintegrator
1-tank with mixer;
2-disperser; 3-air pump
Characterisation
(a)
(b)
Structure of the clay-glass foam:
a) pore structure, b) struts crossection
Compression strength, MPa
Total porosity, %
Glass cullet content, wt.%
5%
7%
10%
Dependence of the compression strength
on the firing temperature and porosity
50 mg/L
100 mg/L
200 mg/L
Intraparticle diffusion kinetic model

Journal of Cleaner Production, Volume 282, February 2021, Article number 124546
DOI: 10.1016/j.jclepro.2020.124546

Influence of waste glass in the foaming process of open cell porous ceramic as filtration media for industrial wastewater

Andrei Shishkin[1], Hakim Aguedal[2,3], Gaurav Goel[4,5*], Julite Peculevica[1], Darryl Newport[6], Jurijs Ozolins[1]

[1]Rudolfs Cimdins Riga Biomaterials Innovations and Development Centre of RTU, Institute of General Chemical Engineering, Faculty of Materials Science and Applied Chemistry, Riga Technical University, Pulka 3, Riga, LV-1007, Latvia.

[2]Laboratoire de Valorisation des Matériaux, Département de Génie des Procédés, Faculté des Sciences et de la Technologie, Université Abdelhamid Ibn Badis – Mostaganem, Bp. 227, 27000 Mostaganem, Algeria.

[3]Laboratoire Ressources Naturelles Sahariennes, Département des Sciences de la Nature et de la Vie, Faculté des Sciences et de la Technologie, Université Ahmed Draia – Adrar 01000, Algeria.

[4]School of Engineering, London South Bank University, SE10AA, United Kingdom.

[5]School of Aerospace, Transport and Manufacturing, Cranfield University, MK430AL, UK

[6]Sustainability Research Institute, University of East London, London E162RD, United Kingdom.

*Corresponding author Email address: goelg@lsbu.ac.uk

Abstract

This paper reports the development and testing results of a prototype ceramic filter with excellent sorption properties (< 99% elimination in 5 min) leading to good efficacy in the removal of industrial contaminants (Reactive Bezaktiv Turquoise Blue V-G (BTB) dye). The novelty in the investigation lies in developing the filter material obtained from the recycling of waste glass combined with highly porous open-cell clay material. This newly developed material showed a significant reduction in the energy requirements (sintering temperature required for the production of industrial filters) thus addressing the grand challenge of sustainable and cleaner manufacturing. The methodology entails sintering of the clay foam (CF) at temperatures ranging from 800 to 1050 °C and blending it with 5%, 7% and 10 wt.% milled glass cullet. One of the aims of this investigation was to evaluate and analyse the effect of the pH of the solution, contact time and equilibrium isotherm on the sorption process and the mechanical compressive strength, porosity, water uptake. From the kinetic studies, it was discovered that the experimental results

were well aligned with the pseudo-second-order model and chemisorption was discovered to be a mechanism driving the adsorption process. These findings are crucial in designing cost-effective industrial filtration system since the filter material being proposed in this work is reusable, recyclable and readily available in abundance. Overall, the pathway for the reuse of waste glass shown by this work help address the sustainability targets set by the UN Charter via SDG 6 and SDG 12.

Keywords: Ceramic clay foam, open cell, sorption capacity, textile dye, isotherm.

1. Introduction

The amount of waste glass, particularly soda-lime glass, is increasing year by year. In the European Union, approximately 16.3 million tons of cullet was collected in 2016 (Eurostat, 2020). There is a pressing need to recyle waste glass and toaddress the theme of waste to wealth. Accordinly, a number of studies have been conducted to use glass cullet as an additional raw material or as a fluxing agent in ceramics (Ondruška et al., 2019)for instance, as a surrogate to natural aggregates, in concrete to build pavements and roads (Majdinasab and Yuan, 2019), and to obtain stoneware tiles and bricks (Chen et al., 2018; Lu et al., 2019; Walczak et al., 2015). The use of cullet, particularly for municipally recycled glass, panel glass, cathode ray tubes has been explored in greater details. Its usage has also been investigated for the manufacturing of glass foams (Silva et al., 2018). Glass foams are produced by combining various foaming agents. Primarily used foaming agents are aluminum nitride, calcium carbonate, silicon carbide and manganese dioxide. The foaming process energy requirement depends on the foaming agent: 700-725 °C for $CaCO_3$ (Bernardo and Albertini, 2006) and 900-1000 °C for SiC (Francis et al., 2013).

In an earlier study glass-ceramics or porous components were manufactured using natural materials and industrial waste, and a compression strength of ~ 80 MPa (Binhussain et al., 2014) was achieved. It has been reported, that the addition of 10 wt.% of waste glass in clay with firing at temperatures of 900-1000°C improved the mechanical traits (Phonphuak et al., 2016) and reduced the firing temperature by 80-100 °C (Shishkin et al., 2020). However, very few studies exist concerning addition of glass (Binhussain et al., 2014; Silva et al., 2018). Taking into account clay-mineral diversity, there is extensive gap in the knowledge relating to clay-cullet mix properties.

With the growing knowledge surrounding the ceramic material with the advantage of their chemical stability, high porousness (Dong et al., 2012), high refractoriness, low mass and thermal conductivity, as well as specific heat (Fukushima and Colombo, 2012), the interest in

these materials is increasing. Work has been done on different aspects such as weight reduction (Goel et al., 2018), improved thermal and acoustic insulation properties (Hostler et al., 2009), application as filters (Song et al., 2006) and catalyst support (Choo et al., 2019). During the past decade, a wide assortment of approaches have been investigated for producing absorbent ceramics, including the replica, the sacrificial template, water-oil emulsion and the direct foaming methods (Colombo, 2008; Yue et al., 2011). However, only one solitary study has been devoted to direct foaming technique despite it being fastest and easiest method (Lakshmi et al., 2015).

Wastewater containing residual dye is produced primarily for textile and leather industries (Yaseen and Scholz, 2019). The treatment technologies utilised at industrial level are either based on activated carbon or Fenton's reagent based method (Wang et al., 2008). These processes are expensive, particulary the regeneration of activated carbon is a tedious and costly operation. In some cases, further treatments are required to purify the water (Durán-Jiménez et al., 2014). So as to overcome the impediments of these technologies, this study proposes porous ceramics as a material for water filtration. Reactive Bezaktiv Turquoise Blue V-G (BTB) dye which is a synthetic anionic dye widely used in the textile industry, was chosen as model organic pollutant. Adsorption of this dye by the designed product was studied and related manufacturing conditions such as firing temperature and glass cullet – Illitic clay mix ratio were analysed.

The overarching aim of this work was to produce clay foam (CF) with high adsorption and adequate compressive strength. The methodology entails sintering of the CF at temperatures ranging from 800 to 1050°C and blending it with 5%, 7% and 10 wt.% milled glass cullet. The novelty in investigation lies in utilizing the waste glass combined with open cell porous clay material that showed significant reduction in the sintering temperature (800°C). This research considered various dye mixed water properties including pH (2-11), contact time (5-300 min), and dye concentration (10-900 $mg \cdot L^{-1}$). Optimum combinations of these factors were determined to maximize the dye adsorption by clay foams, and the mechanisms involved in the process were examined.

The rest of the paper is organised as follows: Section 2 provide details on fabrication technique for clay foam along with batch experiments for dye adsorption. Section 3 details the experimental results and relevant discussions. The paper concludes by highlighting that sorption kinetic process follows the pseudo-second order kinetic model and chemisorption was the dominant mechanism.

2. Materials and methods

Details of materials, fabrication methods, chemical and physical characterization techniques, and batch adsorption experiment details are discussed below.

2.1. Reagents and Raw Materials

The illite type clay (deposition Liepa, Lode JSC, Latvia) was used for foam preparation. This homogenised clay was secured from *Lode* Ltd brick factory (Latvia). The clay agglomerate were dried at 105°C for 24 h, followed by refining in a jaw crusher to yield particle sizes in the range of 10-20 mm. It was then subjected to milling using a laboratory disintegrator DSL-175 (designed at Tallinn Technical University (Estonia) (Zimakov et al., 2007))for obtaining particle sizes < 50 µm. Green bottle glass was used as an milled cullet (MC) source. Clean bottles were fed in jaw crusher, in order to obtain particle size of 10-20 mm. Subsequently they were also milled using the DSL-175 to yield particle sizes < 50 µm. Detailed analysis of chemical and mineralogical composition of the clay and cullet used here can be referenced from our previous work (Shishkin et al., 2020) but some salient details are provided here. Oxide composition of the used clay are: SiO_2 - 62.8 wt%, Al_2O_3 - 15.4 wt%, Fe_2O_3 - 6.8 wt%, CaO - 0.7 wt%, MgO - 1.4 wt%, Na_2O - 0.1 wt%, K_2O - 4.2 wt% TiO_2 - 1.9 wt%; And for MC SiO_2 – 70.2 wt%, Al_2O_3 – 2.1 wt%, Fe_2O_3 - 0.1 wt%, CaO - 9.5 wt%, Na_2O - 16.6 wt%, Fatty alcohol sulfate preparation - Schäumungsmittel W53 Flüssig (Zschimmer & Schwarz GmbH & Co KG Chemische Fabriken, Germany) was used as foaming agent (FA). Municipal utility tap water (Riga, Latvia) and deflocculation agent made of humates and silicates basis Dolaflux B11 (Zschimmer & Schwarz GmbH & Co KG Chemische Fabriken, Germany) were also used for the clay slurry preparation. Phase composition after adding glass was as follows: (i) 800 °C- Quartz, Illite, Haematite, Microcline, Diopside, and amorphous phase (ii) 900 °C- Quartz, Illite, Haematite, Microcline, Diopside, Spinel, Cristobalite, and amorphous phase.

2.2. Mixing and milling

The dry clay and cullet was milled and homogenised using the laboratory disintegrator DSL-175 at a speed of 12000 rpm. Clay foam (CF) was obtained by direct foaming using similar process as reported in previous study (Shishkin et al., 2015) utilising high-speed mixer-disperser device (HSMD) (Corvus Ltd., Riga, Latvia). The core idea of the HSMD is focused on ceramic slurry treatment producing multiple impacts in a liquid medium (cavitation effect) by dispersing elements through the intensive homegenisation thus introducing micro (50-100µm) bubbles (direct foaming) in bulk product.

132 *2.3. CF Production Method*

133 The mix of clay with MC content of 5%, 7%, and 10 wt.% was prepared as the first step.
134 Preparation of the CF comprised of the following stages. The HSMD was operated in
135 circulation mode and set at 500 rpm. It was filled with 600 ml of water and 1 wt.% of dispersant
136 (calculated from dry clay-glass mixture – 14 g). A total of 1400 g dry clay-MC mix was slowly
137 (~300 $g.min^{-1}$) added to prevent agglomeration and the HSMD speed was gradually increased
138 to 4000 rpm. The 5.5 wt.% of foaming agent (calculated from dry clay-glass mixture – 77 g)
139 was added after 30s and the mixer speed was gradually raised to 6000 rpm. With air introduction
140 into the suspension, the foamed mix volume increased twofold. Treatment by HSMD was
141 continued in recirculation mode (1 min). The CF was then fed into a mould of size 150x150x60
142 mm and naturally dried for 72 hours at room temperature. The sample was additionally dried at
143 105°C for 24h. Oven dried sample were removed from the mould, cut into 55x55x110 mm
144 specimens and fired in a muffle furnace (LH11, P330 by Nabertherm) at 900, 950, 1000 and
145 1050 °C at a rate of 5 °C min^{-1} with a dwell time 30 min. The sintered CF samples were cut and
146 polished to a final size of 50x50x50 mm for further tests.
147
148 *2.4. Determination of the Physical and Mechanical Properties*
149 Firing shrinkage was evaluated by direct sizing of the sample's linear dimensions
150 (55x55x110 mm) before and after firing. The water absorption, apparent density, bulk density
151 and apparent porosity were analysed by the pycnometry and Archimedes method (*Annual book*
152 *of ASTM standards, ASTM Standards C20*, 2015). Compressive strength of the sintered
153 specimens (25x25x25mm) were assessed using a Universal Testing Machine (UTM) (Instron
154 8801, Germany) in accordance with ASTM D695. All experiments were organized based on a
155 set of six samples for each category (glass addition and firing temperature) and results reported.
156 For the microstructural characterization, optical microscope (Keyence Corporation, Osaka,
157 Japan, VHX-2000 and VH-Z20R/W lens) was used. Scanning electron microscope (SEM) Zeiss
158 EVO MA-15 (Carl Zeiss AG, Oberkochen, Germany) was used for microstructural
159 characterization at high magnification. High temperature optical microscope (EM201 HT163,
160 Hesse instruments, Germany) was used for optical dilatometry.
161
162 *2.5. Preparation of dye solution*
163 A synthetic dye (BTB), widely used in the textiles industry, was chosen as the targeted
164 pollutant to gauge the sorption capacity of the fabricated specimens and their probable
165 application in industrial wastewater purification. Stock solution was formed by dissolving

exactly weighed amounts (1g) of dye in bi-distilled water to give a strength of 1000 mg· L^{-1}. From this solution, other solutions were prepared by successive dilutions when necessary.

2.6. Batch adsorption experiments

The adsorption experiment was performed by mixing 25 ml of dye solution and 0.65 g of adsorbent. The mixture was shaken at 200 rpm and placed in a centrifuge for 5 minutes at 4000 rpm. The residual concentration of dye was determined by analysis of the supernatant at the wavelength that is consistent to the extreme absorbance, at 625 nm, using UV-visible spectrophotometer (Evolution 300, Thermo Scientific). Portion of adsorbed BTB was as per subsequent equation (1):

$$q_e(\mathrm{mg\cdot g^{-1}}) = \frac{(\mathrm{C_i} - C_e) \times \mathrm{V}}{\mathrm{m}} \qquad (1)$$

where q_e is the quantity of dye adsorbed by bulk of adsorbent (mg·g^{-1}), C_i and C_e are respectively the initial and residual concentration of dye solution (mg·L^{-1}), m is the amount of adsorbent (g), and V is volume of solution (l).

The effect of various factors on the adsorption capacity were examined:

- The outcome of pH on the adsorption capacity, was evaluated by using various pH solutions ranging from 2 to 11. The solutions pH were adjusted by using diluted mix of HNO_3 and NaOH (0.1 N).
- Impact of contact time was studied from 5 to 300 min at three altered initial concentrations 50, 100 and 200 mg·L^{-1}. The obtained kinetic results were modelled by Elovich, Pseudo 1st order, Pseudo 2nd order and intraparticle diffusion kinetic models.
- The effect of initial concentration on dye adsorption capacity was investigated at 20 °C with different dye mixes ranging from 10 to 1000 mg·L^{-1}. Freundlich, Langmuir and Temkin adsorption isotherm were utilized to represent the obtained data from adsorption isotherm study.

3. Results and discussion

Results on clay foam are presented below for their physical, mechanical properties, and adsorption performance.

3.1. Samples and pore morphology

The sample of the CF (MC-7 wt.%), shown in Fig. 1a, had no visible fractures or cracks compared to the CF without MC addition (provided in supplementary information). The

199 microstructure demonstrates (Fig. 2b) an even pore distribution in the sample volume and the
200 presence of interconnected pores which points to an open cell material classification. The
201 sintering process slightly affected the pore size (due to shrinkage), but not the foam morphology
202 where a spherical-like and interconnected open cell microformation was noted for all 12
203 samples series. The average cell diameter for the sintered CF was in the range of 50-200μm and
204 the cell window measurement was 30-70μm (Fig. 1b and 2a). The pore interconnection was
205 formed due to the thin suspension films between the bubbles rupturing during dehydration since
206 the dislocation of powder from the boundary is thermodynamically inimical. The CF walls have
207 a porous structure (Fig. 2b) due to the natural residual clay porosity caused by water evaporation
208 and by formation of lamellar clay structure. The porous walls facilitate the liquid permeability
209 through the structure. The MC addition did not play significant role on the foam morphology
210 and average cell sizes, which were in the 50-200μm range for all samples (5, 7 and 10 wt.% of
211 MC addition).

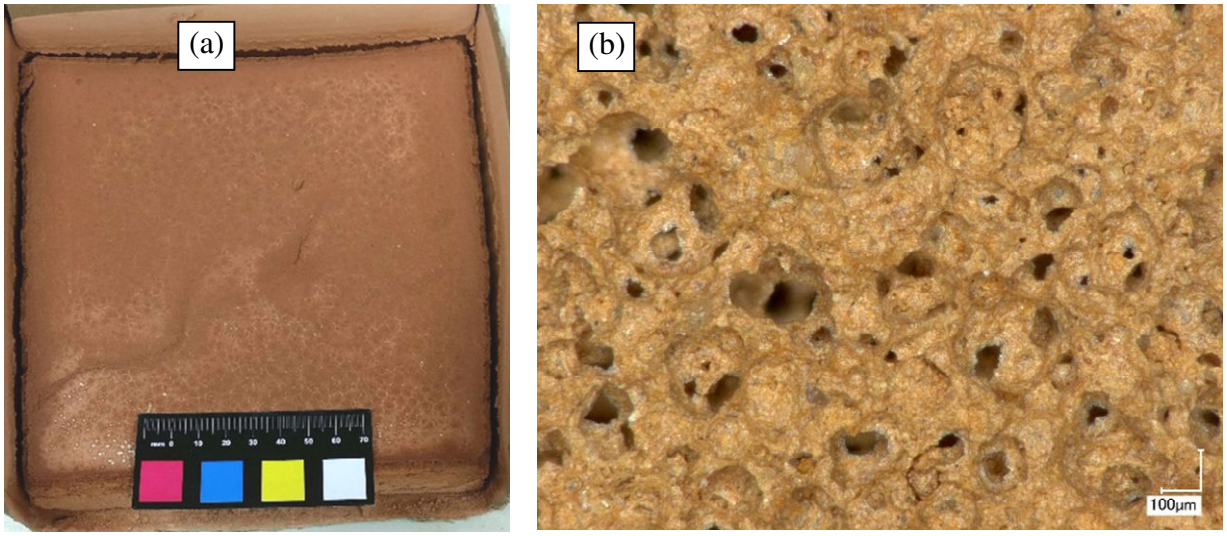

212
213
214 Fig. 1. CF with 7 wt.% MC content. a) green sample after drying; b) fired at 900°C, optical
215 microscope at magnification X200 times.
216

217 According to micro optical observations, with an escalation in the firing temperature the pore
218 sizes decrease by 7-10% for the series sintered at 1050°C in comparison to 900°C. This could
219 be explained by the natural clay shrinkage and densification during the firing.

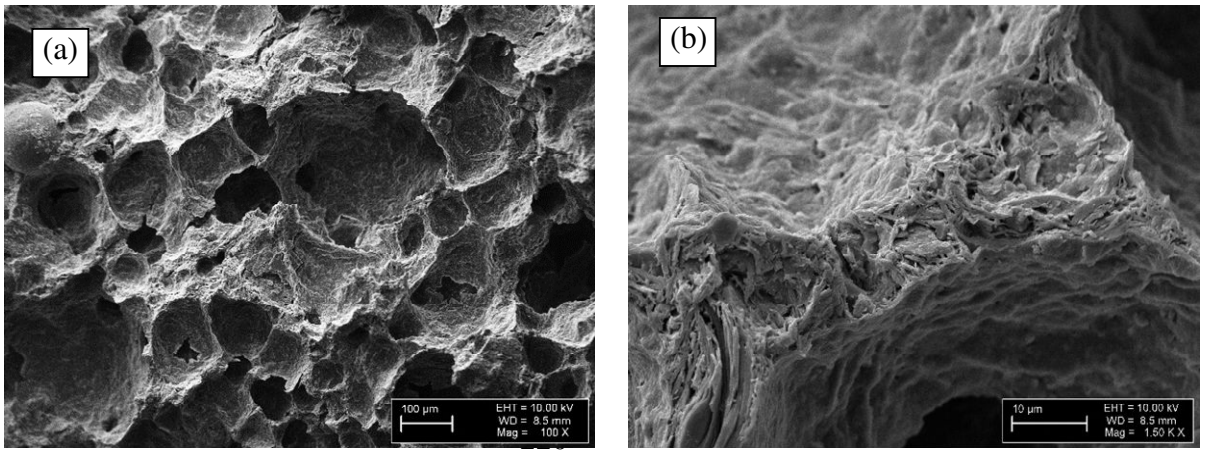

Fig. 2. SEM micrographs of the CF with 7 wt.% MC content, fired at 900°C

3.2. Physical properties

The compressive strength and total porosity of CF samples with diverse MC ratio are presented in Fig. 3. It can be perceived that the porosity augmented by 2-3% with an MC increase from 5 to 7 wt.% (for all sintering temperatures). At the same time, the porosity decreases by 2-2.5% with a firing temperature increase by 50°C for each series. The porosity dependence on the firing temperature exhibited a linear tendency. However, for the firing temperature increase from 950 to 1050 °C, the bulk density showed a steady increase for all compositions, from 0.80 to 0.90 $g \cdot cm^{-3}$, from 0.73 to 0.84 $g \cdot cm^{-3}$, and from 0.66 to 0.75 $g \cdot cm^{-3}$ for 5, 7 and 10 wt.% MC content, respectively. For porous ceramics the bulk density has a direct correlation with shrinkage, the higher the sintering temperature the denser the ceramic particles pack and at the same time pore merging can take place.

Compressive strength increases for all series, with the firing temperature increase. However, the intensity of increase is highly dependent on the MC content. At 900°C clay particles could be bonded and in this case, the amount of MC plays a more significant role. The result of 7 wt.% MC composition shows a higher value of compression strength at 900°C. Overall, the low mechanical properties of 10 wt.% MC sample could be explained by the lower mechanical properties of the glass phase. The total porosity varies almost linearly with sintering temperature increase for all compositions (Fig. 3).

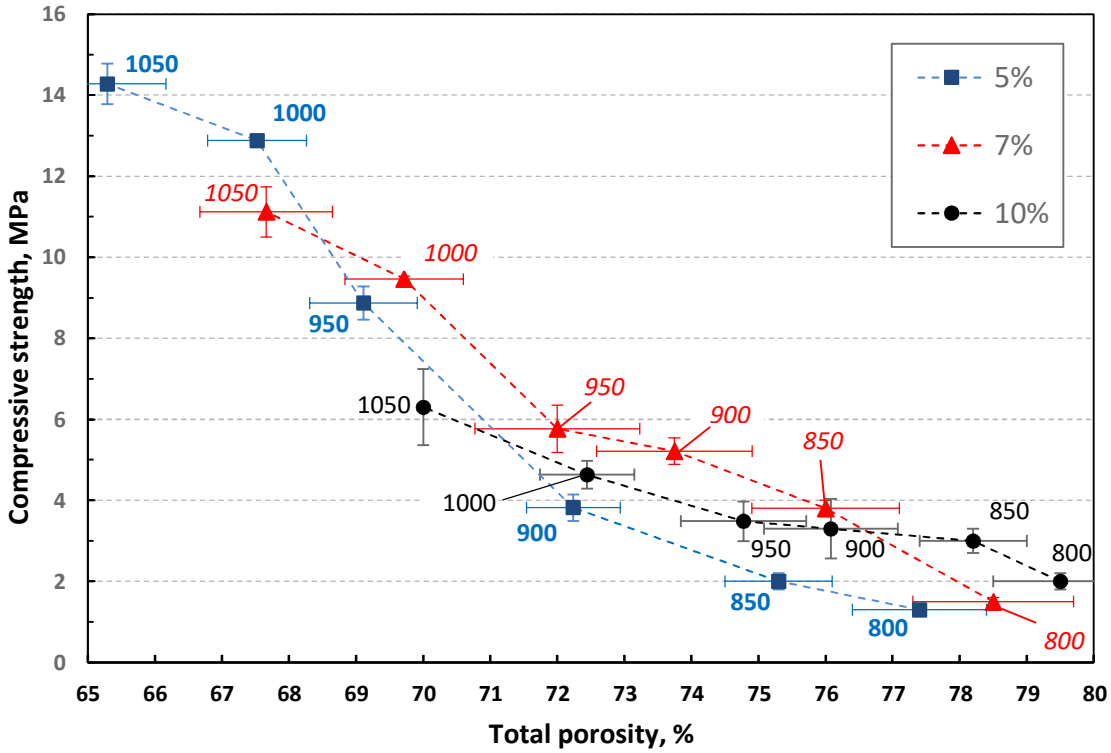

Fig. 3. Dependence of the compressive strength on the firing temperature of samples with 5,7 and 10 wt.% of MC loading at different firing temperatures. MC ratio is indicated in the legend. The firing temperature is indicated in °C.

In view of definite mechanical properties - specific strength (Φ/Δ) is of vital significance in lightweight product design and determination of the best material (Ashby, 2011). From the engineering point of view, lightweight panels could be described and evaluated by specific strength Φ/Δ (MPa·g^{-1}·cm^{-3}) (Novais et al., 2015; Ponsot et al., 2015). However, from an energy efficiency viewpoint it is necessary to consider one more aspect – the temperature and time required for the material production. In the case of investigated natural clay foam with the addition of 5 wt.%, 7 wt.% and 10 wt.% of ground MC, optimal parameters were found for 7 wt.% MC. This composition has the highest compressive strength in the 900°C series - 5.2 MPa. The composition with 5 wt.% MC, sintered at 1000°C has the highest compressive strength in the 1000°C series – 12.9 MPa, and the second highest value of compressive strength (12.6% less than the highest value – 14.3 MPa) in all the series. Therefore composition with 5 wt.% MC, sintered at 1000°C, is better for the construction application (with higher mechanical properties). The record of absolute (MPa) and specific (MPa·g^{-1}·cm^{-3}) strength of the 5-10 wt.% MC loaded clay foam are provided in Table 1.

Table1. The absolute Φ (MPa) and specific Φ/Δ (MPa·g^{-1}·cm^{-3}) strengths of MC-clay foam.

Firing temperature	MC content, wt.%					
	5 wt.%		7 wt.%		10 wt.%	
	Φ	Φ/Δ	Φ	Φ/Δ	Φ	Φ/Δ
800 °C	1.3±0.2	1.9	1.5±0.1	2.3	2.0±0.2	3.6
850 °C	2.0±0.2	2.9	3.8±0.2	5.8	3.0±0.3	5.2
900 °C	3.8±0.3	5.3	5.2±0.3	7.7	3.3±0.7	5.3
950 °C	8.9±0.4	11.1	5.8±0.6	7.9	3.5±0.5	5.3
1000 °C	12.9±0.1	15.3	9.5±0.1	12.0	4.6±0.3	6.5
1050 °C	14.3±0.5	15.8	11.1±0.6	13.2	6.3±0.9	8.4

3.3. Effect of firing and MC content on the adsorption capacity

Preliminary adsorption tests were conducted to evaluate the outcome of firing temperatures (800, 900, 950, and 1000 °C) and glass contents (5, 7 and 10 wt.%).

As demonstrated in Fig. 4, the highest adsorption capacity was observed for samples prepared at relatively low temperatures (800, 900°C) containing 10 wt.% of glass content. The uttermost adsorption capacity registered was 1.7 and 1.8 $mg.g^{-1}$ respectively for MC10-800 and MC10-900. The lowest adsorption capacity was observed at high firing temperatures. Therefore, compositions MC10-800 and MC10-900 were selected as adsorbents for further evaluation of the adsorption process of BTB dye.

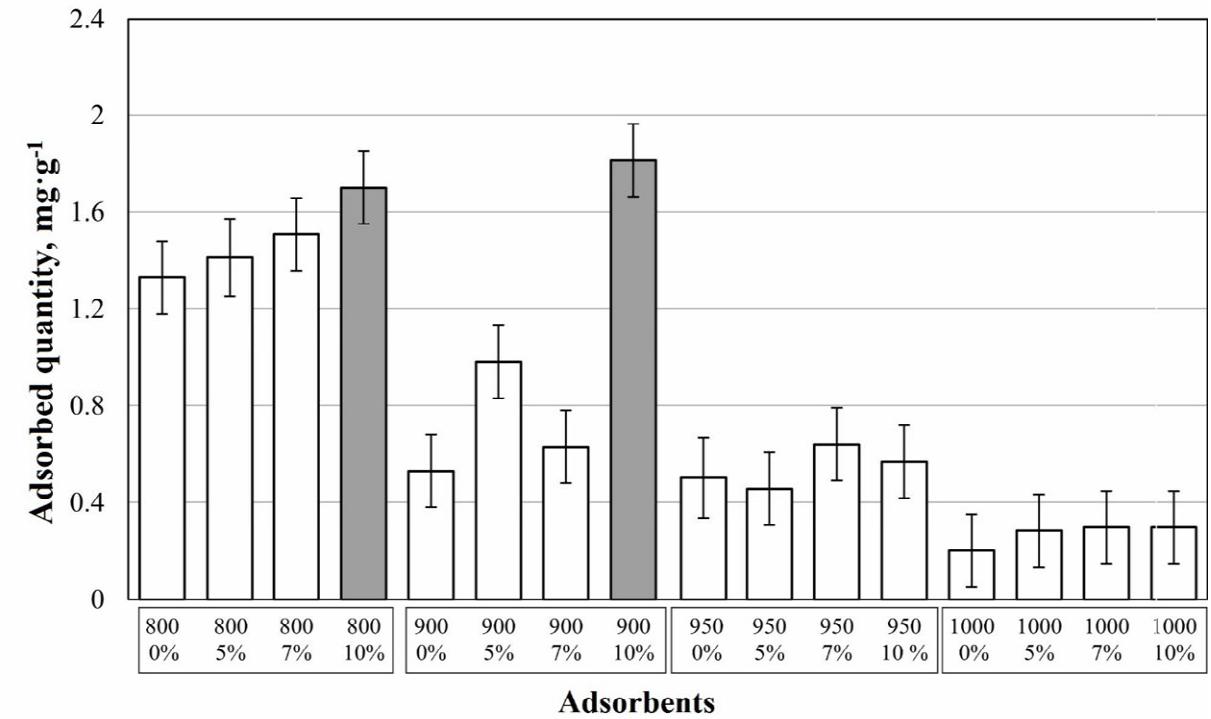

Fig. 4. Preliminary adsorption test of different prepared materials.

3.4. Influence of pH

The pH of mix significantly influences the adsorption capacity of dye onto MC10-800 and MC10-900 as shown in Fig. 5. Indeed, the adsorption capacity augmented when the pH of solution reduced, with the maximum adsorption capacity for both materials being observed at pH 2. Adsorption capacity of 2.4 and 1.7 $mg \cdot g^{-1}$ was obtained, respectively, for MC10-800 and MC10-900. These capacities decreased when the pH of solution increased, achieving the lowest values at pH 5.

As explained by earlier study (Aguedal et al., 2018), the high amount of BTB dye adsorbed onto raw and thermally treated diatomite, in the acidic range, is due to the protonation influence of superficial functional groups of the adsorbents. This effect generates a high electrostatic attraction among the positively charged adsorbent surface and the dye that seems anionic character. However, in the alkaline pH range, hydroxyl ions compete with the molecules of dye to occupy the same available active adsorption sites, which translates into the lowest amount of dye being adsorbed in this range. Hence, a pH 2 is used in the kinetic and isotherm adsorption studies.

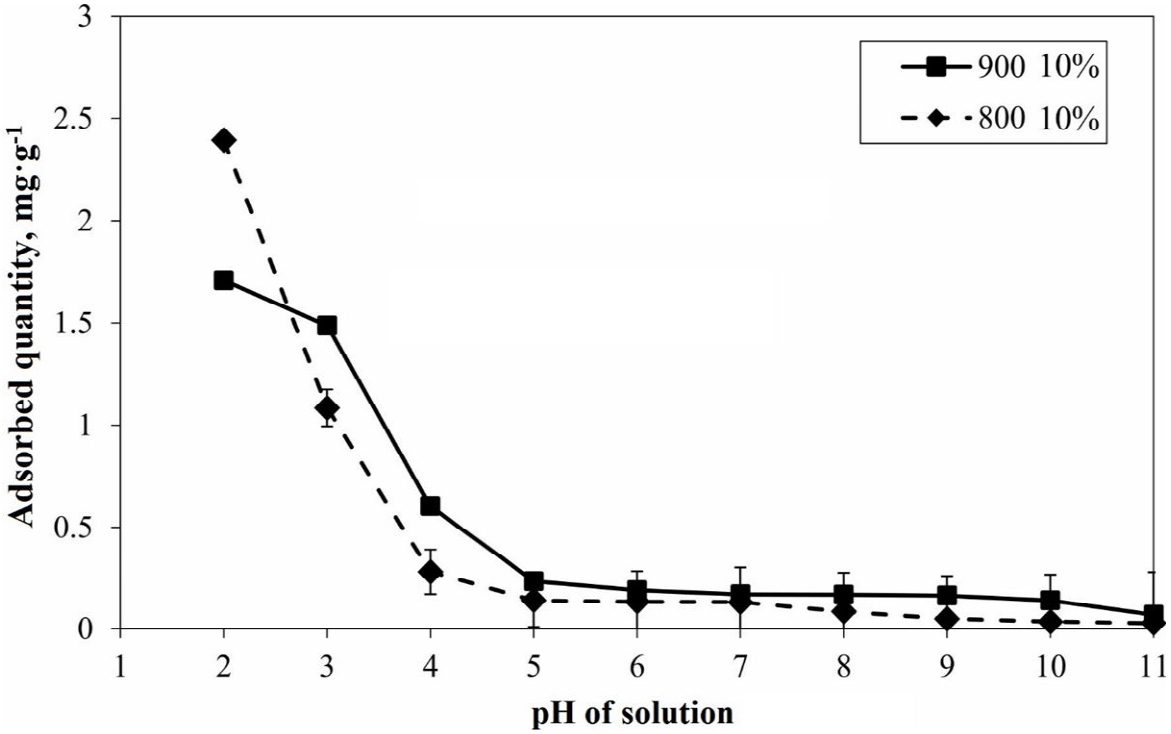

Fig. 5. pH effects on the adsorption capacity of dye at MC10-800 and MC10-900°C.

3.5. Influence of contact time

The rate at which the adsorbent is able to uptake the ascorbate is one of the most significant parameters that governs the appropriateness for the purpose of water quality control. The kinetic

299 study was done to analyse the mechanism and determine the efficiency of the adsorption
300 process. Three concentrations of dye (50, 100 and 200 mg·L^{-1}) were utilized to analyse the
301 adsorption kinetic of BTB dye onto MC10-800 and MC10-900 at different time intervals,
302 between 5 and 300 min, and at an optimised pH. The results are depicted in Fig. 6 and Fig. 7.
303

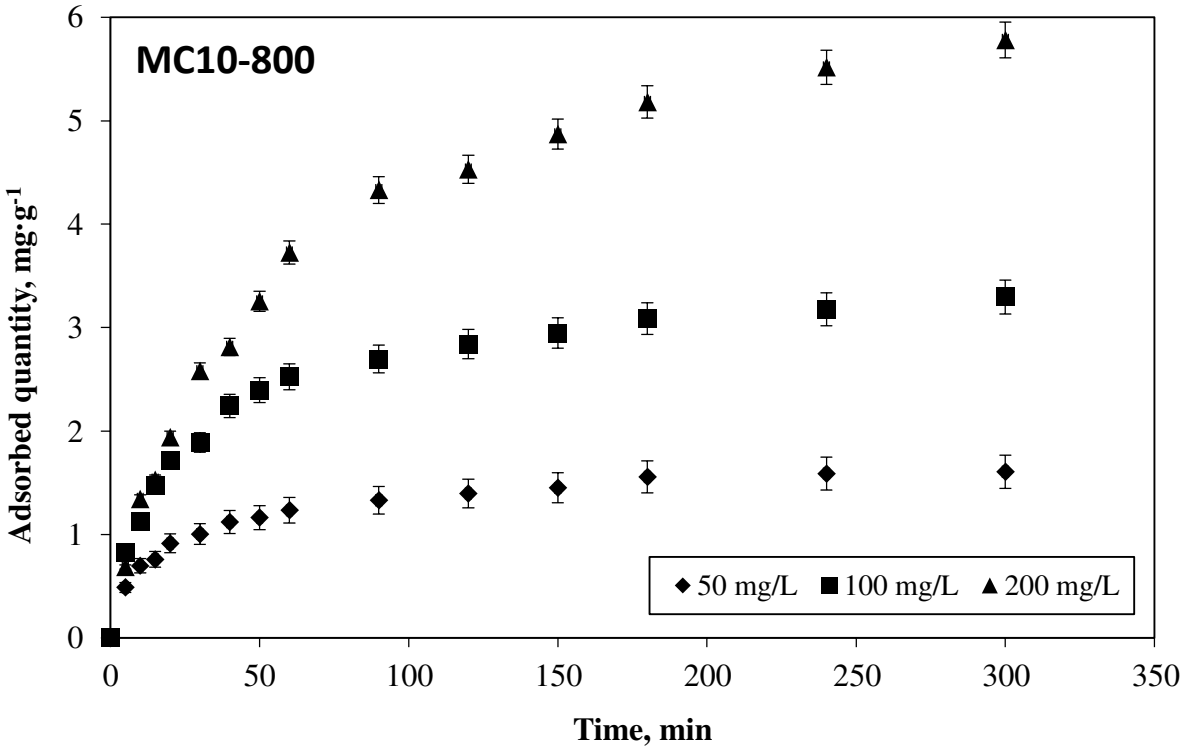

304
305 Fig. 6. Sorption kinetics for MC10-800.

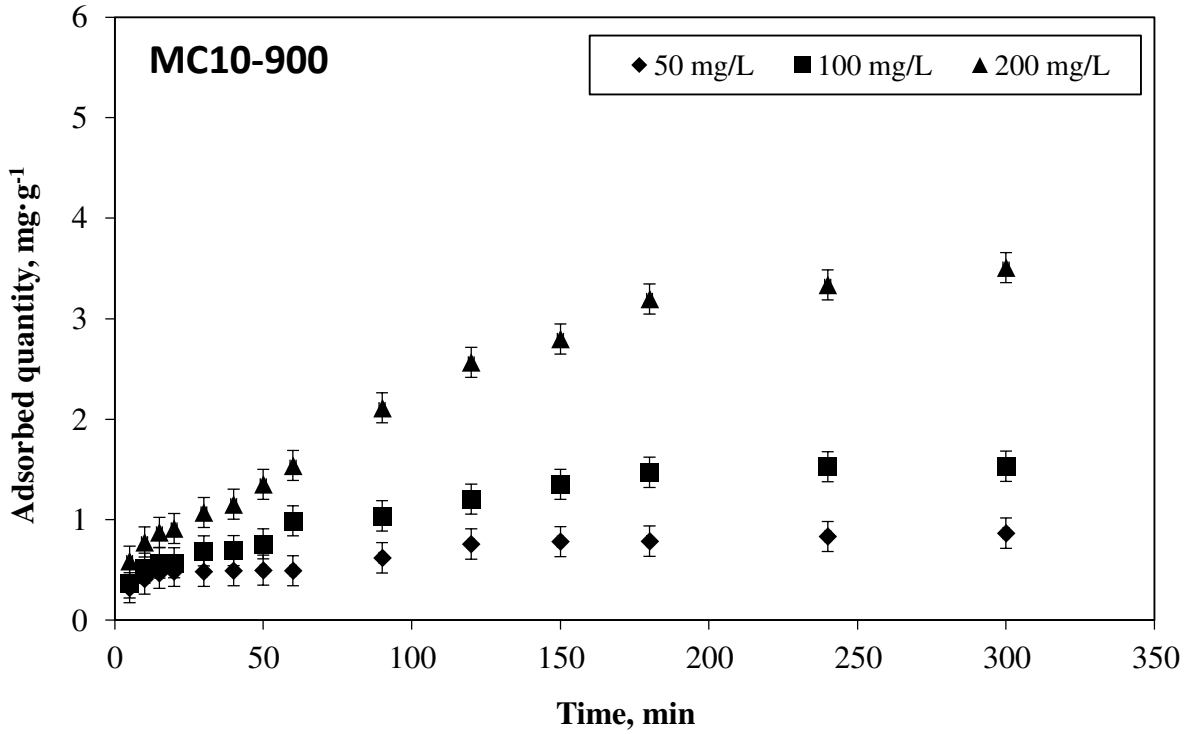

Fig. 7. Sorption kinetics for MC10-900.

It was observed, for all selected dye concentrations, that the adsorption capacity of BTB dye augmented with, surge in contact time and then the adsorption rate reduced and tends towards equilibrium. In addition, the surge in the initial dye concentration increased the exclusion efficiency of dye and significantly increased the equilibrium time. At lower concentrations, the number of available adsorption sites is higher than the number of dye molecules in solution, which lead to equilibrium rapidly. However, at higher concentrations, the amount of dye molecules experiences high gradient of concentration at the liquid-solid interface which increase the deep molecules diffusion to the inner part of MC10-800 and MC10-900 adsorbents, thus explaining the rise in adsorption capacity of dye and equilibrium time (El Haddad et al., 2014). The same observations have been reported in other work (Iddou et al., 2011; Novais et al., 2018).

Adsorption kinetic behaviour of BTB dye onto MC10-800 and MC10-900 was studied using the experimental kinetic specifics and analysed by the Elovitch, pseudo-first order, pseudo-second order and intraparticle diffusion kinetic models (see Table 2). The results of the correlation coefficient and the calculated constant bounds for each model are summarised in Table 3.

Table 2. List of non-linear equations of the used kinetic models and their linearized expressions.

Kinetic models	Equations	Linear expression	Plot	References
Elovich	$q_t = \beta_E \times \ln(\alpha_E \times \beta_E \times t)$	$q_t = \beta \times \ln(\alpha \times \beta) + \beta \times \ln(t)$	q_t vs. ln t	(Zhang and Stanforth, 2005)
Pseudo 1st order	$q_t = q_e [1 - \exp(-k_{1p} \times t)]$	$\ln(q_e - q_t) = \ln(q_e) - k_{1p} \times t$	$\ln(q_e - q_t)$ vs. t	(Aravindhan et al., 2007)
Pseudo 2nd order	$q_t = k_{2p} \times Qe^2 \times t/(1 + k_{2p} \times Q_e \times t)$	$t/q_t = (1/k_{2p} \times q_e^2) + (t/q_e)$	t/q_t vs. t	(Ho and McKay, 1999)
Intra-particle diffusion	$q_t = k_p \times t^{0.5}$	$q_t = k_p \times t^{0.5}$	q_t vs. $t^{0.5}$	(Arami et al., 2008)

q_t and q_e are respectively the adsorbed quantity of dye at time t, and at equilibrium ($mg \cdot g^{-1}$). k_{1p}, k_{2p} and k_p are respectively the kinetic model constant of pseudo-first order (min^{-1}), pseudo-second order ($g \cdot mg^{-1} \cdot min^{-1}$) and intraparticle diffusion ($g \cdot mg^{-1} \cdot min^{-0.5}$); α ($mg \cdot g^{-1} \cdot min^{-1}$) and β ($g \cdot mg^{-1}$) are the Elovich kinetic model constants.

From the high values of correlation coefficient R^2, the adsorption kinetics of BTB dye are well matched by the pseudo-second order kinetic model for all adsorbents. In addition, the calculated adsorption capacities by this model are similar to those obtained in batch mode test (see Fig. 8 and Fig. 9).

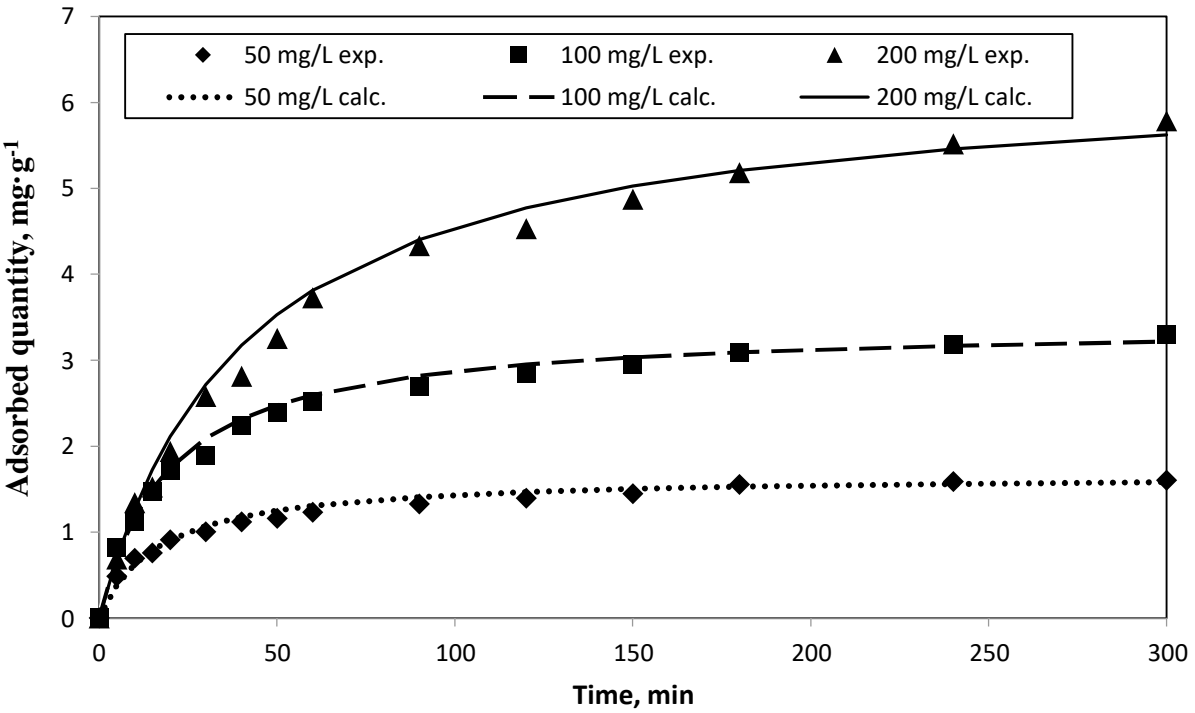

Fig. 8. The adsorption amount of dye onto MC10-800 obtained experimentally and fitted pseudo-second order kinetic model.

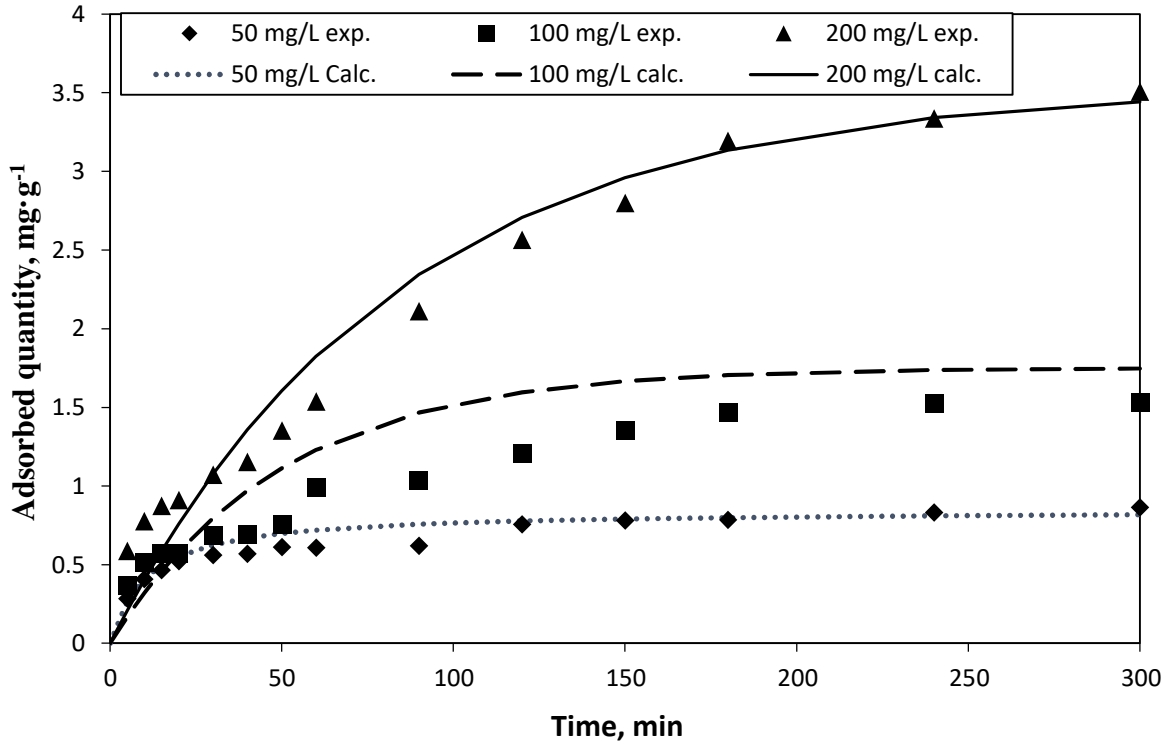

Fig. 9. The adsorption amount of dye onto MC10-900 obtained experimentally and fitted pseudo-second order kinetic model.

Matching of experimental results to the pseudo-second order kinetic model indicates that the chemisorption could be the rate-controlling step on the first stage as well as at low concentrations. However, the assumption of molecular diffusion could be one more mechanism involved in the removal process of BTB dye onto MC10-800 and MC10-900, which is justified using intraparticle diffusion kinetic model. Indeed, as reported by Weber and Morris (W. Weber, J. Morris, 1963), if intraparticle diffusion is the dominant step in the adsorption method of BTB dye onto MC10-800 and MC10-900, then a plot of q_t versus $t^{0,5}$ ought be linear and advance along the origin (Behnamfard and Salarirad, 2009). From Fig. 10a and Fig. 10b it can be seen that the plot is often multilinear (two linear steps) signifying that the intraparticle diffusion is by no means the rate-limiting step for the entire adsorption process. The initial linear step confirms the fast adsorption during the first time of contact. As the reaction constant for the intraparticle diffusion k_p increase with the initial dye concentration, the slowdown in the second stage is certainly owing to the resistance diffusion of dye molecules into the interior adsorption available sites (Bhatti and Nausheen, 2014).

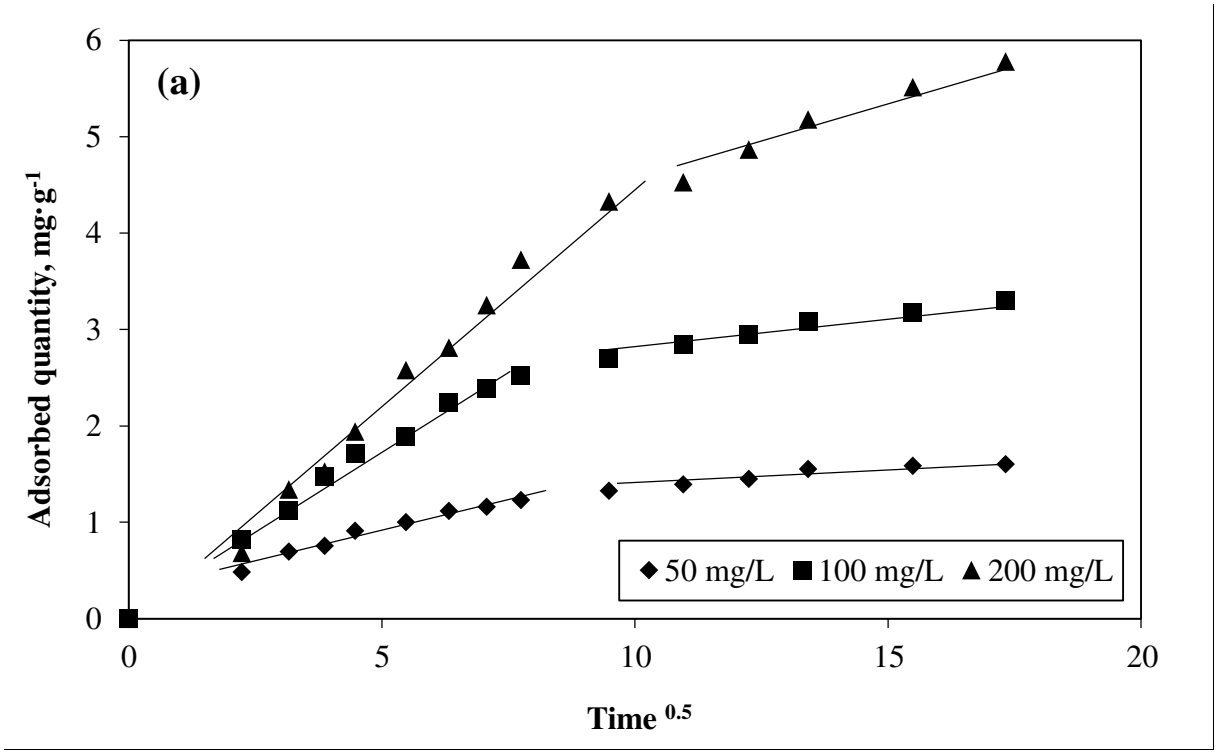

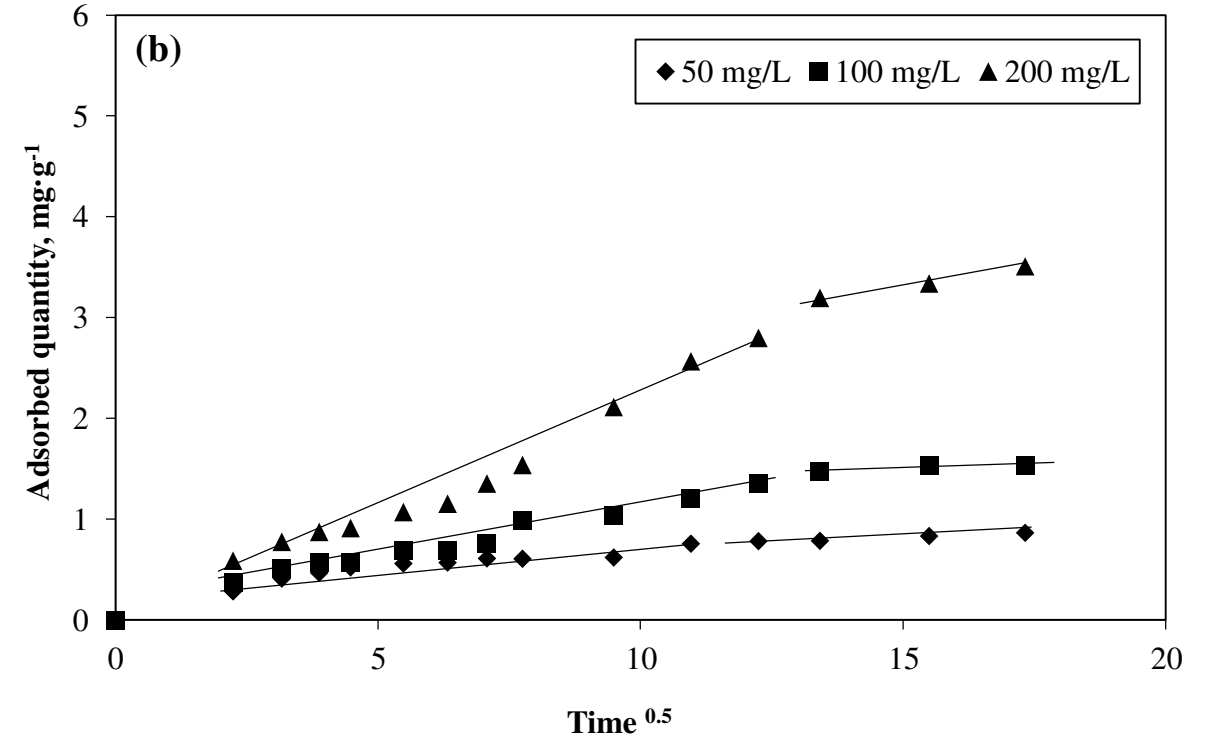

Fig. 10 Intraparticle diffusion kinetic model plots of BTB dye adsorption at different initial concentration onto (a) MC10-800, (b) MC10-900.

Table 3. Kinetic model parameters for MC10-800 and MC10-900 samples.

Kinetics model	Parameters	MC10-800			MC10-900		
		50 mg·L^{-1}	100 mg·L^{-1}	200 mg·L^{-1}	50 mg·L^{-1}	100 mg·L^{-1}	200 mg·L^{-1}
Elovich	β	0.288	0.61	1.136	0.14	0.28	0.66
	α	3.76	1.94	0.37	9.67	1.97	0.52
	R^2	0.996	0.991	0.953	0.98	0.93	0.86
Pseudo-first order	q_e	1.28	2.11	4.961	0.53	1.75	3.53
	k_{1p}	0.017	0.013	0.012	0.012	0.02	0.012
	R^2	0.945	0.928	0.96	0.94	0.89	0.98
Pseudo-second order	q_e	1.67	3.42	6.38	0.88	1.68	4.1
	k_{2p}	0.036	0.015	0.004	0.067	0.017	0.003
	R^2	0.995	0.995	0.983	0.99	0.97	0.91
Interparticle diffusion	k_p	0.038	0.177	0.352	0.041	0.09	0.22
	R^2	0.861	0.871	0.954	0.85	0.96	0.98

3.6. Adsorption isotherm

The adsorption equilibrium isotherm was assessed by studying the outcome of initial dye concentration at room temperature and optimized value of pH and contact time (pH = 2, equilibrium time of 2h). Tests were performed at varying dye concentrations from 10 to 900 mg·L^{-1}. Fig. 11a and Fig.11b depict, that the rise in the early dye concentration causes a rapid growth in the amount of dye adsorbed onto MC10-800 and MC10-900, and gradually increases until the equilibrium and/or saturation state of MC10-800 and MC10-900 adsorbent is reached. The same phenomenon was observed by Kousha et al (2012). As reported by Novais et al (2018), that the mass transfer resistances at the solid-liquid interface is overcome by increasing the preliminary dye concentration, which provide significant driving force enhancing the adsorption process. Hence, a higher initial concentration could lead to adsorbent saturation.

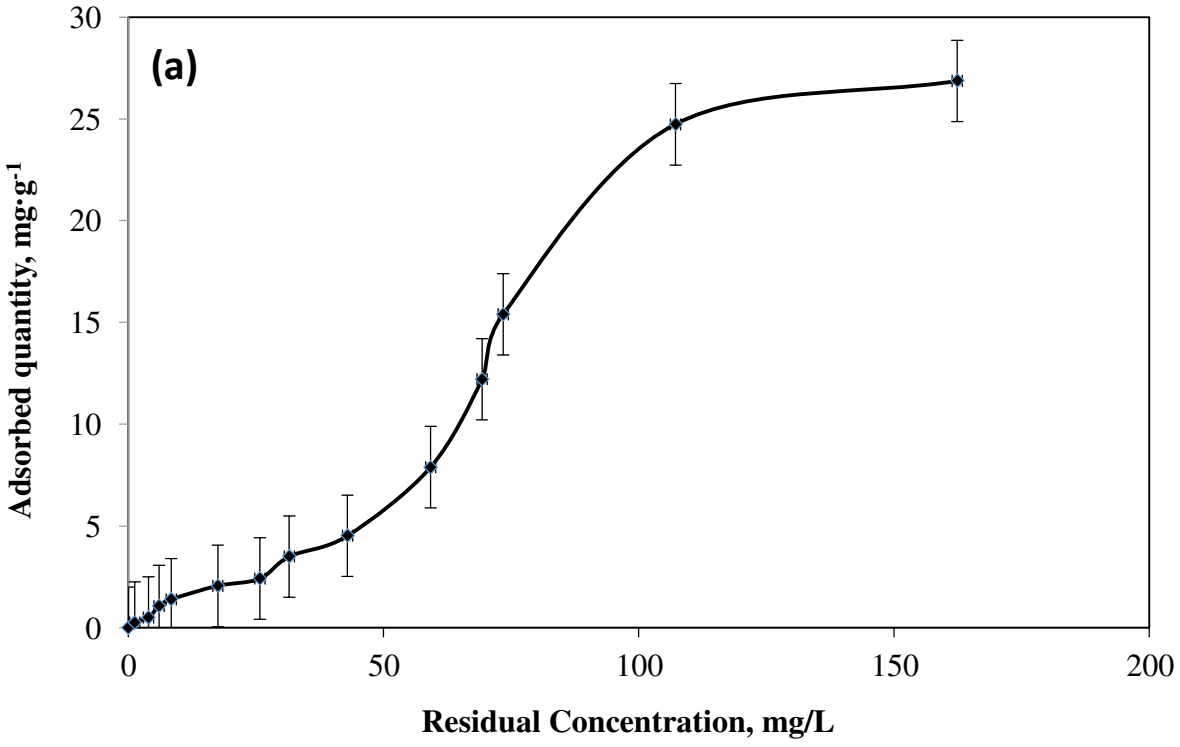

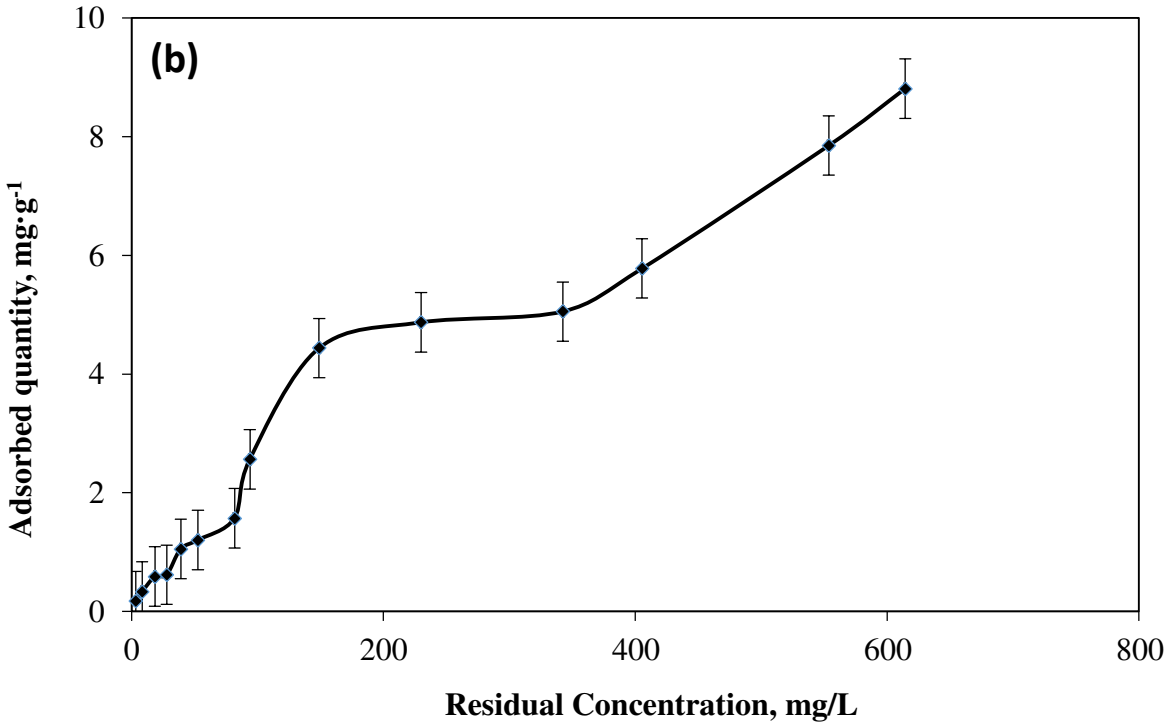

Fig. 11. Effect of initial dye concentration (a) MC10-800 and (b) MC10-900.

Equilibrium isotherm equations characterize the adsorption mechanism of BTB dye onto MC10-800 and MC10-900 adsorbents. Observed data were fitted by Langmuir, Freundlich and Temkin isotherm model (see Table 4). In order to decide if the isotherm model is suitable to describe the experimental results, high correlation coefficients (R^2) for the best fitting isotherm model can be refereed. Table 5 summarises all the correlation coefficient R^2 values obtained from each of the models applied in the adsorption study of BTB dye onto MC10-800 and MC10-900.

Table 4: List of non-linear equations of the used isotherm models and their linearized expressions.

Isotherm model	Equations	Linear expression	Plot	References
Freundlich	$q_e = K_F \times (C_e)^{1/n}$	$\ln (q_e) = \mathrm{Ln}\ (K_F) + (\ln (C_e)/n)$	ln (qe) vs. ln (Ce)	(Chan et al., 2012)
Langmuir	$q_e = (K_L \times Q_m \times C_e) / (1 + K_L \times C_e)$	$1/q_e = (1/K_L \times q_m \times C_e) + (1/q_m)$	$1/q_e$ vs. $1/C_e$	(Secula et al., 2011)
Temkin	$q_e = q_m \times \ln (K_T \times C_e)$	$q_e = q_m \times \ln (K_T) + q_m \times \ln (C_e)$	q_e vs. ln (C_e)	(Behnamfard and Salarirad, 2009)

q_e (mg·g^{-1}) and C_e (mg·L^{-1}) are respectively the equilibrium adsorbed quantity and equilibrium concentration, K_F (mg·g^{-1}) Freundlich isotherm constant (mg·g^{-1}), 1/n Freundlich exponent, q_m (mg·g^{-1}) maximal adsorption quantity, K_L (L·mg^{-1}) Langmuir isotherm constant, K_T (L·mg^{-1}) Temkin isotherm constant.

Table 5. The isotherm model parameters for MC10-800 and MC10-900.

Isotherm model	Parameters	MC10-800	MC10-900
Freundlich	K_F	0.28	0.19
	n	1.19	1.82
	R^2	0.87	0.76
Langmuir	K_L	0.023	0.018
	q_m	8.80	3.16
	R^2	0.97	0.96
Temkin	K_T	0.28	9.98
	q_m	4.36	1.32
	R^2	0.60	0.75

From Table 5, it may be perceived that the adsorption isotherm data of BTB dye onto MC10-800 and MC10-900 are best matched by the Langmuir isotherm model giving the highest R^2 comparing to Freundlich and Temkin models. Underpinning the Langmuir assumptions, the adsorption molecules of BTB dye onto MC10-800 and MC10-900 occurred in monolayer at a homogeneous adsorbent surface. Thus chemisorption is the main mechanism controlling the whole adsorption process (Caner et al., 2009).

The increasing sorption ability of the MC10-800 material can be explained by the high porosity of CF due to a lower firing temperature. This is supported by the high temperature microscopy results (Fig. 12a and 12b), where it is clearly visible that at temperature above 860°C, the glass changed from solid conditions, corresponding to low-viscosity state and transfers into a semi-liquid phase. At 900 °C glass has much lower viscosity. Beyond 900 °C glass addition promotes Liepa clay sintering, which decreases porosity and increases shrinkage which in good correlation with obtained strength-porosity results for studied porous ceramics in this research.

This is supported by the dilatometry measurements which demonstrated a rapid increase of the shrinkage (Fig. 12a) after 860°C. At the same time, at 860°C, the glass completely transferred to semi-liquid conditions (Fig. 12b) and started working as a ceramic particle binder. Thereby, conditions are optimum at 800°C for MC utilisation with maximum porosity and results in maximum adsorption in the specimen.

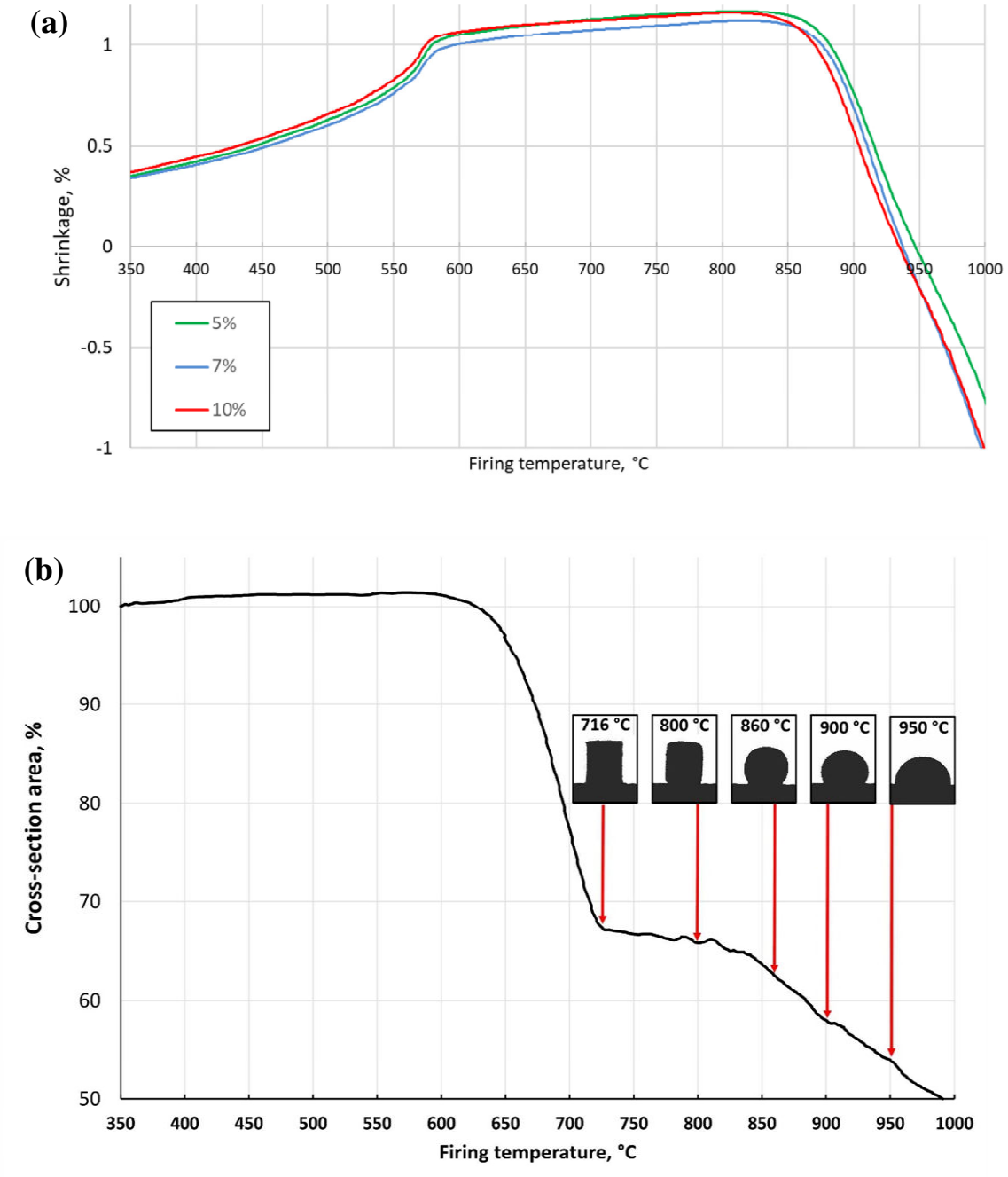

Fig. 12. (a) Dilatometry measurements of the MC5, MC7, MC10 (b) high-temperature microscopy measurements of the glass prism cross-section during firing.

3.7. Benchmarking of results and possible mechanism of dye adsorption

Removal of BTB with other adsorbents used by other researchers has been compared in Table 6. Values reported in the table implies that adsorption capacity achieved in this study is comparable with other studies in literature. However it may be noticed while others materials

(e.g. activated carbon) are carbon based and may be for single use whereas ceramic material obtained in this work can be reused for several cycles after thermal treatment or it can be used as construction material (Petrella et al., 2018). Thus, it is cost efficient and environment friendly.

Table 6. Removal of the BTB dye with different adsorbents as reported in literature.

Adsorbent	Adsorption capacity ($mg.g^{-1}$)	Reference
MC10-800	26.8	Present study
Diatomite [a]	27.8	(Aguedal et al., 2018)
Activated sludge	38.2	(Djafer et al., 2016)
Chitosan/zeolite A	305.8	(Nešic et al., 2013)
Brown macroalga	35.6	(Kousha et al., 2012)
Pine Cone	37.4	(Mahmoodi et al., 2011)
Humin immobilized on silica	19.4	(Jesus et al., 2011)
Activated carbons [b]	66.8	(Ahmad and Rahman, 2011)
Anaerobic sludge	117.1	(Caner et al., 2009)
	100.0	(Kargi and Ozmıhcı, 2005)
Activated carbons [c]	3.4	(Amin, 2008)
Chitosan-crosslinked beads	30.0	(Kimura et al., 2002)

[a] : Treated at 600°C
[b] : Prepared from coffee husk
[c] : Prepared from bagasse pith

Based on literature and according to the effect of pH on the adsorption process, possible scheme of the BTB dye adsorption mechanism on the fired clay-glass surface is as follows. All the reactive dyes behaves similarly in aqueous media (Awasthi et al., 2020). As noticed from molecular structure of BTB dye (Fig. 13), it will be ionized in aqueous solution, by the presence of sulfonate group (SO^{3-}) groups and the rupture of the OH bond leading to an overall negative charged aqueous solution. On the other hand, in acidic range, the protonation effect conduct to charge positively all the functional groups on the surface of ceramic clay (Al-Ghouti et al., 2009). Hence, a strong electrostatic attraction is created between the dye molecules and the surface of ceramic clay according to the scheme (Fig. 14). Once, bonds structure is occupied, further links could occur between the dye molecules via intermolecular attraction such as Van der Waals and hydrogen bonds (Ahmed and Jhung, 2017). Additionally, the O−H or oxygen bonds present on CF (Yang et al., 2020) may probably form an n−π bonding with the aromatic ring of BTB dye (Olusegun and Mohallem, 2020). The decrease of the adsorption capacity at high pH is due to, at alkaline range, the hydroxyl ions will be adsorbed strongly on the active

site onto ceramic clay competing thereby with the BTB dye molecules, hence leading to the high repulsive interactions for the BTB dye molecules (Awasthi et al., 2020).

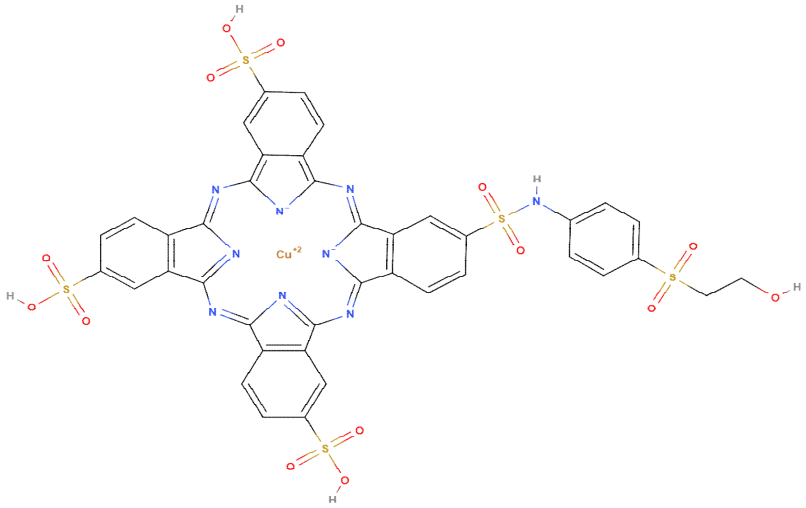

Fig. 13. BTB dye chemical structure (ChemicalBook, 2020).

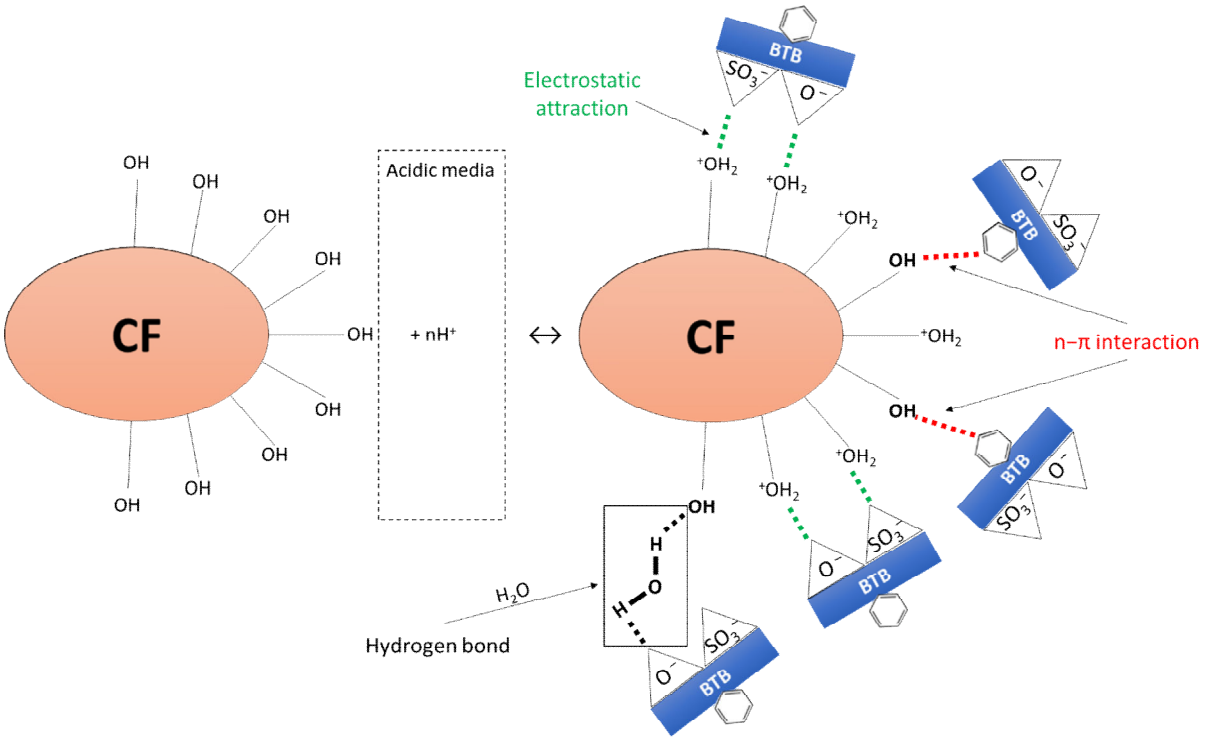

Fig. 14. Scheme of the possible adsorption process mechanism.

Conclusion

This novel multidisciplinary research paper reports experimental aspects involved in the development of new material (potentially useful as a component of industrial water filtration system). The material fabricated is highly porous clay ceramic foam containing cullet and is

obtained by direct foaming and cavitation disperser. Due to the relatively simple technology of ceramic clay foam production, with careful technological development, the technological uptake of the method is sustainable and it addresses the pressing international need of bringing environmental-friendliness in industrial production. Future development of the clay-glass ceramics should be directed towards lowering of firing temperature below 800 °C and improved glass milling efficiency to obtain finer particles with higher specific surface area to achieve greater sorption ability.

During this investigation, it was discovered that the mechanical properties improve with the increasing glass content and perform best when the fired temperature is in the range of 800-900°C. Other broad conclusions drawn were as follows:

- Benchmarking done against the published literature showed the newly proposed material possess a desirable adsorption capacity of 26.8 $mg.g^{-1}$ comparable to other research materials developed and reported to date. Furthermore, the open cell ceramic foam promotes a cleaner alternative.
- Experimental results indicated that the glass transferred to liquid phase above 860°C and started promoting intensive bonding with ceramic particles. This bonding contributes towards higher compressive strength at higher sintering temperatures.
- A pH value of 2 was found most optimal to attain the maximum adsorption capacities of up to 13%. The equilibrium time was affected by the intensification in the initial dye concentration.
- The sorption kinetic process followed the pseudo-second order kinetic model, indicating potential chemical relations between the sorbent and the sorbate. The Langmuir isotherm model described the experimental results well compared to other empirical models. Thus, chemisorption was discovered to be the driving mechanism controlling the adsorption process.

Acknowledgements:

The authors would like to thank Faculty of Materials Science and Applied Chemistry, Riga Technical University for providing the facilities. We express thanks to the STSM support from Cost Action CA17133 (funded by H2020) to enable the UK-Latvian collaboration. GG is particularly thankful to the Royal Academy of Engineering, UK to extend financial support via

the Indo-UK partnership Industry-academia scheme (Grant No. IAPP18-19\295) with a follow-on funding under the auspices of the Engineering Pandemic preparedness program (EXPP2021\1\277). GG also acknowledge financial support from the European Regional Development Funds (ERDF) sponsored A2i project at LSBU that have catalysed several industrial partnerships. All authors are very thankful to the EU wide Cost Actions CA18224, CA18220, CA17136 and CA18125 supported by H2020.

Bibliography

Aguedal, H., Iddou, A., Locs, J., 2018. Optimization of the Adsorption Process of Bezaktiv Turquoise Blue « VG » Textile Dye onto Diatomite Using the Taguchi Method 762, 81–86. https://doi.org/10.4028/www.scientific.net/KEM.762.81

Ahmad, M.A., Rahman, N.K., 2011. Equilibrium, kinetics and thermodynamic of Remazol Brilliant Orange 3R dye adsorption on coffee husk-based activated carbon. Chem. Eng. J. 170, 154–161. https://doi.org/10.1016/j.cej.2011.03.045

Ahmed, I., Jhung, S.H., 2017. Applications of metal-organic frameworks in adsorption/separation processes via hydrogen bonding interactions. Chem. Eng. J. 310, 197–215. https://doi.org/10.1016/j.cej.2016.10.115

Al-Ghouti, M.A., Al-Degs, Y.S., Khraisheh, M.A.M., Ahmad, M.N., Allen, S.J., 2009. Mechanisms and chemistry of dye adsorption on manganese oxides-modified diatomite. J. Environ. Manage. 90, 3520–3527. https://doi.org/10.1016/j.jenvman.2009.06.004

Amin, N.K., 2008. Removal of reactive dye from aqueous solutions by adsorption onto activated carbons prepared from sugarcane bagasse pith. Desalination 223, 152–161. https://doi.org/10.1016/j.desal.2007.01.203

Annual book of ASTM standards, ASTM Standards C20, 2015. , Standard Test Methods for Apparent Porosity, Water Absorption, Apparent Specific Gravity, and Bulk Density of Burned Refractory Brick and Shapes by Boiling Water.

Arami, M., Limaee, N., Mahmoodi, N., 2008. Evaluation of the adsorption kinetics and equilibrium for the potential removal of acid dyes using a biosorbent. Chem. Eng. J. 139,

2–10.

Aravindhan, R., Rao, J.., Nair, B.., 2007. Removal of basic yellow dye from aqueous solution by sorption on green alga Caulerpa scalpelliformis. J. Hazard. Mater. 142, 68–76. https://doi.org/https://doi.org/10.1016/j.jhazmat.2006.07.058

Ashby, M.F., 2011. Designing Hybrid Materials, in: Materials Selection in Mechanical Design. Elsevier, pp. 299–340. https://doi.org/10.1016/B978-1-85617-663-7.00011-4

Awasthi, A., Arya, A., Gupta, P., Kumar, R., Singh, J., Datta, D., 2020. Adsorption of Reactive Blue-13, an Acidic Dye, from Aqueous Solution Using Magnetized Activated Carbon. J. Chem. Eng. Data 65, 2220–2229. https://doi.org/10.1021/acs.jced.0c00081

Behnamfard, A., Salarirad, M.M., 2009. Equilibrium and kinetic studies on free cyanide adsorption from aqueous solution by activated carbon. J. Hazard. Mater. 170, 127–133. https://doi.org/10.1016/j.jhazmat.2009.04.124

Bernardo, E., Albertini, F., 2006. Glass foams from dismantled cathode ray tubes. Ceram. Int. 32, 603–608. https://doi.org/10.1016/j.ceramint.2005.04.019

Bhatti, H.N., Nausheen, S., 2014. Equilibrium and kinetic modeling for the removal of Turquoise Blue PG dye from aqueous solution by a low-cost agro waste. Desalin. Water Treat. 1–11. https://doi.org/10.1080/19443994.2014.927799

Binhussain, M.A., Marangoni, M., Bernardo, E., Colombo, P., 2014. Sintered and glazed glass-ceramics from natural and waste raw materials. Ceram. Int. 40, 3543–3551. https://doi.org/10.1016/j.ceramint.2013.09.074

Caner, N., Kiran, I., Ilhan, S., Iscen, C.F., 2009. Isotherm and kinetic studies of Burazol Blue ED dye biosorption by dried anaerobic sludge. J. Hazard. Mater. 165, 279–284. https://doi.org/10.1016/j.jhazmat.2008.09.108

Chan, L.., Cheung, W.., Allen, S.., McKay, G., 2012. Error Analysis of Adsorption Isotherm Models for Acid Dyes onto Bamboo Derived Activated Carbon. Chinese J. Chem. Eng. 20, 535–542. https://doi.org/https://doi.org/10.1016/S1004-9541(11)60216-4

ChemicalBook, 2020. Reactive Turquoise Blue [WWW Document]. BTB Dye. URL https://www.chemicalbook.com/ProductChemicalPropertiesCB1874871_EN.htm (accessed 7.23.20).

Chen, Z., Li, J.S., Poon, C.S., 2018. Combined use of sewage sludge ash and recycled glass cullet for the production of concrete blocks. J. Clean. Prod. 171, 1447–1459. https://doi.org/https://doi.org/10.1016/j.jclepro.2017.10.140

Choo, T.F., Mohd Salleh, M.A., Kok, K.Y., Matori, K.A., 2019. Modified cenospheres as non-sacrificial pore-forming agent for porous mullite ceramics. Ceram. Int. 45, 21827–21834. https://doi.org/10.1016/j.ceramint.2019.07.189

Colombo, P., 2008. Engineering porosity in polymer-derived ceramics. J. Eur. Ceram. Soc. 28, 1389–1395. https://doi.org/10.1016/j.jeurceramsoc.2007.12.002

Djafer, A., Djafer, L., Maimoun, B., Iddou, A., Mostefai, S.K., Ayral, A., 2016. Reuse of waste activated sludge for textile dyeing wastewater treatment by biosorption : performance optimization and comparison 1–8. https://doi.org/10.1111/wej.12218

Dong, Y., Wang, C.-A., Zhou, J., Hong, Z., 2012. A novel way to fabricate highly porous fibrous YSZ ceramics with improved thermal and mechanical properties. J. Eur. Ceram. Soc. 32, 2213–2218. https://doi.org/10.1016/j.jeurceramsoc.2012.03.016

Durán-Jiménez, G., Hernández-Montoya, V., Montes-Morán, M.A., Bonilla-Petriciolet, A., Rangel-Vázquez, N.A., 2014. Adsorption of dyes with different molecular properties on activated carbons prepared from lignocellulosic wastes by Taguchi method. Microporous Mesoporous Mater. 199, 99–107. https://doi.org/10.1016/j.micromeso.2014.08.013

El Haddad, M., Regti, A., Slimani, R., Lazar, S., 2014. Assessment of the biosorption kinetic and thermodynamic for the removal of safranin dye from aqueous solutions using calcined mussel shells. J. Ind. Eng. Chem. 20, 717–724. https://doi.org/10.1016/j.jiec.2013.05.038

Eurostat, 2020. Treatment of waste by waste category, hazardousness and waste management operations [WWW Document]. URL https://appsso.eurostat.ec.europa.eu/nui/submitViewTableAction.do

Francis, A.A., Abdel Rahman, M.K., Daoud, A., 2013. Processing, structures and compressive properties of porous glass-ceramic composites prepared from secondary by-product materials. Ceram. Int. 39, 7089–7095. https://doi.org/10.1016/j.ceramint.2013.02.048

Fukushima, M., Colombo, P., 2012. Silicon carbide-based foams from direct blowing of polycarbosilane. J. Eur. Ceram. Soc. 32, 503–510. https://doi.org/10.1016/j.jeurceramsoc.2011.09.009

Goel, G., Kalamdhad, A.S., Agrawal, A., 2018. Parameter optimisation for producing fired bricks using organic solid wastes. J. Clean. Prod. 205, 836–844. https://doi.org/10.1016/j.jclepro.2018.09.116

Ho, Y.S., McKay, G., 1999. Pseudo-second order model for sorption processes. Process Biochem. 34, 451–465. https://doi.org/10.1016/S0032-9592(98)00112-5

Hostler, S.R., Abramson, A.R., Gawryla, M.D., Bandi, S.A., Schiraldi, D.A., 2009. Thermal conductivity of a clay-based aerogel. Int. J. Heat Mass Transf. 52, 665–669. https://doi.org/10.1016/j.ijheatmasstransfer.2008.07.002

Iddou, A., Hadj Youcef, M., Aziz, A., Ouali, M.S., 2011. Biosorptive removal of lead (II) ions from aqueous solutions using Cystoseira stricta biomass: Study of the surface modification effect. J. Saudi Chem. Soc. 15, 83–88. https://doi.org/10.1016/j.jscs.2010.10.007

Jesus, A.M.D., Romão, L.P.C., Araújo, B.R., Costa, A.S., Marques, J.J., 2011. Use of humin as an alternative material for adsorption/desorption of reactive dyes. Desalination 274, 13–21. https://doi.org/10.1016/j.desal.2011.01.063

Kargi, F., Ozmıhcı, S., 2005. Comparison of adsorption performances of powdered activated sludge and powdered activated carbon for removal of turquoise blue dyestuff. Process Biochem. 40, 2539–2544. https://doi.org/10.1016/j.procbio.2004.11.003

Kimura, I.Y., Laranjeira, M.C.M., de Fávere, V.T., Furlan, L., 2002. The interaction between reactive dye containing vinylsulfone group and chitosan microspheres. Int. J. Polym. Mater. 51, 759–768. https://doi.org/10.1080/714975829

Kousha, M., Daneshvar, E., Sohrabi, M.S., Jokar, M., Bhatnagar, A., 2012. Adsorption of acid orange II dye by raw and chemically modified brown macroalga Stoechospermum marginatum. Chem. Eng. J. 192, 67–76. https://doi.org/10.1016/j.cej.2012.03.057

Lakshmi, V., Resmi, V.G., Raju, A., Deepa, J.P., Rajan, T.P.D., Pavithran, C., Pai, B.C., 2015. Concentration dependent pore morphological tuning of kaolin clay foams using

sodium dodecyl sulfate as foaming agent. Ceram. Int. 41, 14263–14269. https://doi.org/10.1016/j.ceramint.2015.07.056

Lu, J.-X., Zheng, H., Yang, S., He, P., Poon, C.S., 2019. Co-utilization of waste glass cullet and glass powder in precast concrete products. Constr. Build. Mater. 223, 210–220. https://doi.org/https://doi.org/10.1016/j.conbuildmat.2019.06.231

Mahmoodi, N.M., Hayati, B., Arami, M., Lan, C., 2011. Adsorption of textile dyes on Pine Cone from colored wastewater: Kinetic, equilibrium and thermodynamic studies. Desalination 268, 117–125. https://doi.org/10.1016/j.desal.2010.10.007

Majdinasab, A., Yuan, Q., 2019. Post-consumer cullet and potential engineering applications in North America. Resour. Conserv. Recycl. 147, 1–9. https://doi.org/https://doi.org/10.1016/j.resconrec.2019.04.009

Nešic, A.R., Velicˇkovic, S.J., Antonovic, D.G., 2013. Modification of chitosan by zeolite A and adsorption of Bezactive Orange 16 from aqueous solution. Compos. Part B 53, 145–151.

Novais, R.M., Caetano, A.P.F., Seabra, M.P., Labrincha, J.A., Pullar, R.C., 2018. Extremely fast and efficient methylene blue adsorption using eco-friendly cork and paper waste-based activated carbon adsorbents. J. Clean. Prod. 197, 1137–1147. https://doi.org/10.1016/j.jclepro.2018.06.278

Novais, R.M., Seabra, M.P., Labrincha, J.A., 2015. Lightweight dense/porous bi-layered ceramic tiles prepared by double pressing. J. Mater. Process. Technol. 216, 169–177. https://doi.org/10.1016/j.jmatprotec.2014.09.010

Olusegun, S.J., Mohallem, N.D.S., 2020. Comparative adsorption mechanism of doxycycline and Congo red using synthesized kaolinite supported CoFe2O4 nanoparticles. Environ. Pollut. 260, 114019. https://doi.org/10.1016/j.envpol.2020.114019

Ondruška, J., Csáki, Š., Štubňa, I., 2019. Influence of waste glass addition on thermal properties of kaolin and illite, in: Central European Symposium on Thermophysics 2019 (Cest). p. 020028. https://doi.org/10.1063/1.5120158

Petrella, A., Spasiano, D., Rizzi, V., Cosma, P., Race, M., De Vietro, N., 2018. Lead Ion Sorption by Perlite and Reuse of the Exhausted Material in the Construction Field. Appl.

Sci. 8, 1882. https://doi.org/10.3390/app8101882

Phonphuak, N., Kanyakam, S., Chindaprasirt, P., 2016. Utilization of waste glass to enhance physical–mechanical properties of fired clay brick. J. Clean. Prod. 112, 3057–3062. https://doi.org/10.1016/j.jclepro.2015.10.084

Ponsot, I., Bernardo, E., Bontempi, E., Depero, L., Detsch, R., Chinnam, R.K., Boccaccini, A.R., 2015. Recycling of pre-stabilized municipal waste incinerator fly ash and soda-lime glass into sintered glass-ceramics. J. Clean. Prod. 89, 224–230. https://doi.org/10.1016/j.jclepro.2014.10.091

Secula, M.S., Cagnon, B., Creţescu, I., Diaconu, M., Petrescu, S., 2011. Removal of an acid dye from aqueous solutions by adsorption on a commercial granular activated carbon: Equilibrium, kinetic and thermodynamic study. Sci. Study Res. Chem. Chem. Eng. Biotechnol. Food Ind.

Shishkin, A., Baronins, J., Mironovs, V., Lukáč, F., Štubňa, I., Ozolins, J., 2020. Influence of Glass Additions on Illitic Clay Ceramics. Materials (Basel). 13, 596. https://doi.org/10.3390/ma13030596

Shishkin, A., Korjakins, A., Mironovs, V., 2015. Using of Cavitation Disperser, for Porous Ceramic and Concrete Material Preparation. Int. J. Environ. Chem. Ecol. Geol. Geophys. Eng. 9, 511–515.

Silva, R. V., de Brito, J., Lye, C.Q., Dhir, R.K., 2018. The role of glass waste in the production of ceramic-based products and other applications: A review. J. Clean. Prod. 167, 346–364. https://doi.org/10.1016/j.jclepro.2017.08.185

Song, I.H., Kim, M.J., Kim, H.D., Kim, Y.W., 2006. Processing of microcellular cordierite ceramics from a preceramic polymer. Scr. Mater. 54, 1521–1525. https://doi.org/10.1016/j.scriptamat.2005.12.039

W. Weber, J. Morris, and J.S., 1963. Kinetics of adsorption carbon from solutions. J. Sanit. Eng. Div. 89, 31–38.

Walczak, P., Małolepszy, J., Reben, M., Rzepa, K., 2015. Mechanical Properties of Concrete Mortar Based on Mixture of CRT Glass Cullet and Fluidized Fly Ash. Procedia Eng. 108, 453–458. https://doi.org/https://doi.org/10.1016/j.proeng.2015.06.170

Wang, X., Zhu, N., Yin, B., 2008. Preparation of sludge-based activated carbon and its application in dye wastewater treatment. J. Hazard. Mater. 153, 22–27. https://doi.org/10.1016/j.jhazmat.2007.08.011

Yang, Q., Yu, H., He, Y., Liu, Z., Qin, C., Liu, B., Li, Y., 2020. Porous three-component hybrid hydrogen-bonded covalent organic polymers: Design, synthesis and ciprofloxacin adsorption. Eur. Polym. J. 123, 109445. https://doi.org/10.1016/j.eurpolymj.2019.109445

Yaseen, D.A., Scholz, M., 2019. Textile dye wastewater characteristics and constituents of synthetic effluents: a critical review. Int. J. Environ. Sci. Technol. 16, 1193–1226. https://doi.org/10.1007/s13762-018-2130-z

Yue, N., Xue, M., Qiu, S., 2011. Fabrication of hollow zeolite spheres using oil/water emulsions as templates. Inorg. Chem. Commun. 14, 1233–1236. https://doi.org/10.1016/j.inoche.2011.04.029

Zhang, J., Stanforth, R., 2005. Slow Adsorption Reaction between Arsenic Species and Goethite (α-FeOOH): Diffusion or Heterogeneous Surface Reaction Control. Langmuir 21, 2895–2901.

Zimakov, S., Goljandin, D., Peetsalu, P., Kulu, P., 2007. Metallic powders produced by the disintegrator technology. Int. J. Mater. Prod. Technol. 28, 226. https://doi.org/10.1504/IJMPT.2007.013081